DOI: 10.1007/s10297-006-0078-0
Originally published in J. Opt. Fiber. Commun. Rep. 4, 214–224 (2007)

All-weather long-wavelength infrared free space optical communications

D.P. Hutchinson and R.K. Richards

Engineering Science and Technology Division
Oak Ridge National Laboratory
Bethel Valley Road, Oak Ridge, TN 37831

Abstract. Long-wavelength infrared radiation possesses superior transmission through common atmospheric problems such as fog, clouds, and smoke than the shorter wavelength laser sources in use today. Recent improvements in LWIR laser and modulator design makes possible reliable optical replacements for radio and microwave communications links in many applications. This paper describes components and techniques developed for high-speed, full-duplex all-weather infrared communications systems.

1. Introduction

Long-wavelength infrared radiation possesses better all-weather transmission than the shorter wavelength laser sources in use today. The superior transmission through common atmospheric problems such as fog, clouds, and smoke coupled with improvements in LWIR laser and modulator design makes possible reliable optical replacements for radio and microwave communications links in many applications Another advantage of LWIR laser radiation is the inherent eye safety of this wavelength region. To take advantage of the transmission characteristics of infrared radiation in the atmosphere, we have developed components for a high-speed, full-duplex all-weather infrared communications link for ranges up to 12 km. In support of this program, we have designed and constructed a compact, RF-driven waveguide CO_2 laser and a dielectric-waveguide Stark modulator. The modulator is based on the Stark shift of NH_2D (deuterated ammonia). The laser is an RF-driven waveguide design.

2. Atmospheric Transmission: The Case for LWIR

Transmission of optical radiation through the atmosphere is reduced by molecular absorption and aerosol extinction (absorption + scattering). Absorption and scattering are highly wavelength dependent phenomenon. For this reason, selecting a laser wavelength may be the most important variable when considering a given communications application. This section on atmospheric transmission includes four subsections that we feel are the most important aspects to consider for an infrared communications and/or lidar application on the battlefield. The first subsection, molecular absorption, uses the well known HITRAN [1] database to show the atmospheric transmission superiority of the $^{13}C^{16}O_2$-isotope wavelengths ($\sim$10.8 μm) over the standard $^{12}C^{16}O_2$ laser wavelengths ($\sim$10.6 μm). The remainder of the subsections deal with aerosols. Aerosols, particles suspended in the atmosphere, broadly encompass everything from microscopic dust to macroscopic fog droplets. A baseline continental aerosol extinction model is presented, then smoke and fog are covered individually. Aerosol extinction models for CO_2 wavelengths are plotted in comparison to visible, and when possible, 1.55 μm wavelengths. The aerosol extinction coefficients available for the standard $^{12}CO_2$ wavelengths are assumed to be representative of the $^{13}CO_2$ isotope wavelengths as well. Owing to the numerous possible combinations of variables within each subsection one or two representative graphs will be provided and trends and exceptions will be noted in the paragraphs.

2.1. *Molecular Absorption Model*

The molecular absorption study was conducted with the computer program HITRAN-PC [2]. The transmission calculations, shown in Figs. 1 and 2, were preformed with the 1976 U.S. Standard for partial pressures of the constituent gases in air. The roundtrip path length used in the calculations is 12 km. The calculations used a standard pressure of 1 atm and temperature of 296°K. Figure 1 shows the atmospheric transmission around the standard $^{12}C^{16}O_2$ laser wavelengths. The most intense P (20) line at 10.59 μm only provides a 40% transmission. Other nearby laser lines are also shown in Fig. 1, and a similar reduction in radiation intensity is also experienced due to the natural abundance of $^{12}C^{16}O_2$ in the atmosphere. Figure 2 shows a very promising alternative, the $^{13}C^{16}O_2$-isotope. The three specific laser lines shown in Fig. 2 are the R(20), R(18), and R(16) at the wavelengths of 10.768, 10.784, and 10.80 μm, respectively. Each of these laser lines provides more than 80% transmission over a total distance of 12 km at the given conditions.

In addition, a few of the other R-branch transitions of this isotope also provide over 95% transmission.

2.2. *Smoke Extinction Model*

The smoke extinction model employed in this subsection is built around optical theory of small particles that group together to form larger particles. For the sake of clarity, the small particles will be referred to as spherules and the larger particles will be referred to as clusters. Each of these clusters has a fractal dimension, which describes how well packed the individual spherules are within the cluster. A minimum fractal dimension of

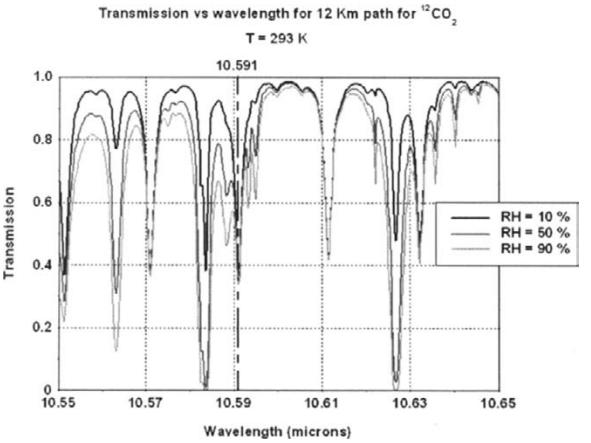

Fig. 1. Atmospheric transmission for a 12-km range.

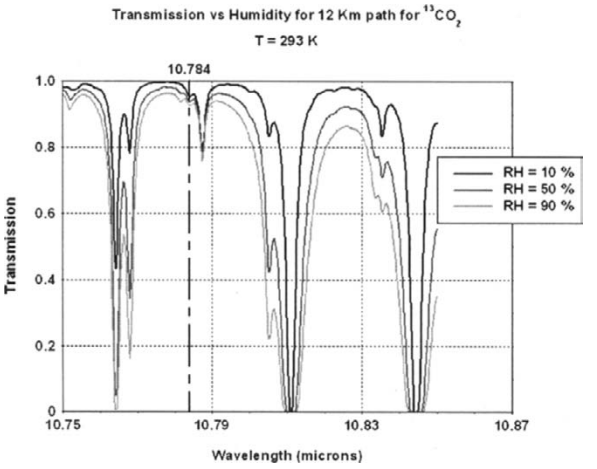

Fig. 2. Transmission of three lines for the Carbon-13 isotope of carbon dioxide.

1 refers to an array of just barely touching spherules, and a maximum fractal dimension of 3 refers to a totally compact cluster with no voids. A fractal dimension, D, of 1.78 has been accepted for smoke [3]. The average number of individual spherules in each cluster is given by [4]:

$$N = (R/a)D, \tag{1}$$

where R is the average cluster radius and a is the average spherule radius.

The absorption cross-sections were calculated for vector waves [4]:

$$\sigma_a = 4\pi N k a^3 \mathrm{Im}[(M^2 - 1)/(M^2 + 2)], \tag{2}$$

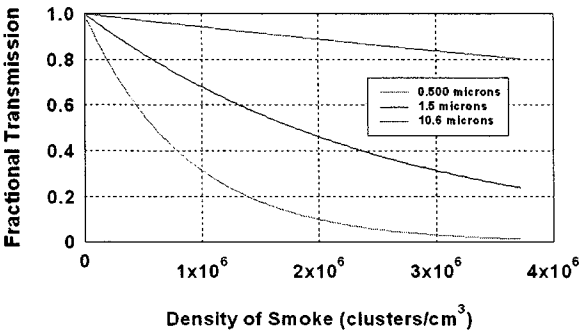

Fig. 3. Comparison of transmission through smoke.

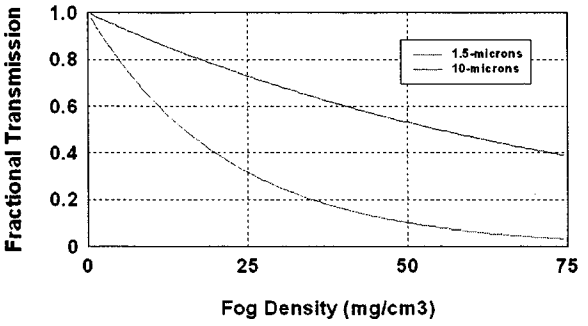

Fig. 4. Fractional transmission of 1.5 and 10 μm light through 100 m of fog.

where $k = 2\pi/\lambda$ and M is the complex index of refraction at wavelength λ.

The transmission of radiation is calculated:

$$T = e^{-\sigma\rho L}, \tag{3}$$

where σ is the extinction cross-section, ρ is the density, and L is the total path length. The average spherule radius is around 0.01 μm [4]. For smoke the absorption cross-section is much larger than the scattering cross-section, thus σ_a can be taken as a good estimate of the extinction cross-section σ.

Figure 3 shows the transmission of 10-μm, 1.5-μm, and 500-nm radiation versus smoke density. The total path length is 1000 m. All calculations are for a cluster size of R =0.1 μm. The indices of refraction used for smoke particles for 10-μm and 500-nm were $M_{10} = 3 + i$ and $M_{0.5} = 1.75 + .3i$, respectively [4]. Since Berry and Percival did not provide an index at 1.5 μm for soot particles one was calculated by using the same value as for visible light, i.e., $M_{1.5} \approx M_{0.5} = 1.75 + .3i$.

Other sources report smoke particle size within the range of 0.005–0.15 μm range [4]. This reduction in cluster size would correspondingly yield much longer path

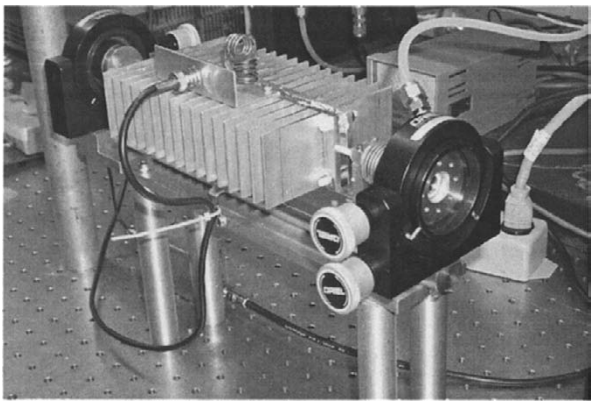

Fig. 5. Air-cooled, RF-driven CO_2 Laser.

lengths (for all wavelengths), but the wavelength trends shown in Fig. 3 will stay the same. With this in mind, Fig. 3 is best used as a relative comparison of the superiority of 10-μm to visible and 1.5-μm radiation.

2.3. Fog Extinction Model

The estimate for extinction of 10- and 1.5-μm radiation by fog is shown in Fig. 4. These extinction coefficients were obtained from graphical data presented in Rensch and Long [5]. The extinction coefficients for 10- and 1.5-μm radiation were 0.55 and 2.0 (dB/km)/(mg/m^3), respectively. The extinction coefficient chosen above from Rensch and Long for 10-μm seems to agree within 10% with the experimentally measured coefficients in Chimelis [3,6]. The average water droplet radius for the fog is 1 μm and the path length is 100 m.

3. Component Development for LWIR Communications

3.1. Compact RF-Driven Laser

One of the drawbacks to more widespread applications for long wavelength infrared communications systems is an inexpensive, compact source of 10-μm radiation. We have developed a compact CW RF-driven, air-cooled, sealed-off waveguide CO_2 laser featuring a power level of over 1 W. The hollow Al_2O_3 ceramic waveguide has an i.d. of 2.4-mm and provides a gain length of 20 cm. Our waveguide laser is based on a design reported by Walsh [7]. A photograph of the laser is shown in Fig. 5. This laser produces a power level of approximately 1.6 W using $^{12}CO_2$ and 0.8 W using $^{13}CO_2$, both in the EH_{11} dielectric waveguide mode. With a grating installed, our laser produces 0.4 W on the 10.59-μm line of $^{12}CO_2$. The output mode structure of the laser, measured with a thermally sensitive liquid crystal film, appears to be a TEM_{00}

Gaussian mode. Frequency measurements indicate that the laser operates in a single transverse and single longitudinal mode.

The gas mixture in the laser is He:CO_2:N_2:CO in the ratio of 65:18:15:2, respectively. This is a commercial mixture purchased for a pulsed CO_2 laser and the composition has not yet been optimized for our CW waveguide laser. Walsh used a mixture of He:CO_2:N_2:Xe in the mixture ratio 77:10:10:3, respectively.

One end of the laser cavity consists of a 0.5-in.-diameter, 3-m-radius concave ZnSe 95% reflective output coupler attached to the waveguide through a brass bellows. The ceramic waveguide is attached with epoxy to a brass fitting soldered to the bellows. Epoxy is also used to attach a ZnSe Brewster window is to the other end of the ceramic tube, which was ground to the Brewster's angle. A 150 l/mm flat master grating mounted on a piezoelectric actuator in an adjustable mirror mount forms the other end of the cavity. A 1-in.-diameter invar rod machined flat on opposing sides serve as a temperature stable mounting surface for the insulating support for the electrodes and the mirror mounts. The optimum operating pressure of the sealed-off laser is 60–65 torr. The laser is driven by a 58.5-MHz RF amplifier at a power level of approximately 50 W. Machined aluminum heatsinks are mechanically clamped to each side of the waveguide serve as RF electrodes and provide cooling for the tube. The two electrodes are shaped to conform to the round dielectric waveguide. A thin coating of heatsink compound applied to the electrodes during assembly improves thermal contact with the dielectric waveguide and enhances cooling. One side of the electrode is grounded and an air wound autotransformer couples RF power to the other electrode. The inductance of the 4-turn autotransformer resonates with the capacitance formed by the heatsinks attached to the waveguide at a frequency of 58.5 MHz. Another air-core inductor is used to connect the 50-Ω coaxial cable from the RF power supply to a tap (approximately 1-turn from the grounded end) on the autotransformer to efficiently couple power to the laser. The inductance of the coupling coil is adjusted by compressing or expanding the coil to optimize the impedance match to the 50-Ω cable. Both coils are constructed from #12 AWG copper wire.

3.2. *Stark-Effect Modulator*

Stark-effect modulation occurs when an electric field is applied to a gas molecule that has a substantial polarization. The applied electric field effectively changes the energy spacing of the molecular levels changing the optical frequency or wavelength that is absorbed by the gas. Also, the energy spacing is very small compared to the energy of the optical photon interacting with the gas. The modulator is filled with approximately 2 or more torr of partially deuterated ammonia (NH_2D), which has a molecular absorption resonance near the 10.59-μm wavelength line of emission of a CO_2 laser. The frequency difference between the absorption resonance and the laser line is reported to be approximately 2189-MHz [8] from the laser line. The dotted curve in Fig. 6 depicts the transmission of a 30-cm cell containing 2-torr of NH_2D in the absence of an applied electric field. The laser light (located at zero difference frequency on the scale) is not strongly absorbed by the cell. The solid curve in the left graph in Fig. 6 shows the transmission of the same cell in the presence of an applied electric field of 300 V/mm. The electric field causes this absorption line to split into nine Stark components classified by the designation $M = 0, \pm 1, \pm 2, \pm 3$, and ± 4. The $M = 0$ component is roughly in the center of the plot at a difference frequency of

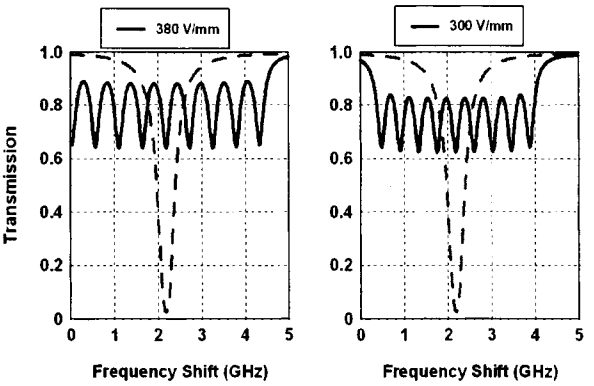

Fig. 6. The application of an electric field to deuterated ammonia causes the absorption peak to split into nine components.

2189 MHz and the $M = \pm 4$ components are at the extreme left and right ends of the structure. As the electric field is increased the $M = \pm 4$ absorption component moves closer to zero difference frequency until the peak of the absorption is in coincidence with the laser line corresponding to an electric field of approximately 380 V/mm. This situation is depicted in left graph shown in Fig. 6. As the applied electric field is varied from 350 to 380 V/mm, the transmission of the 30-cm-long cell varies from 90% to 75%. If the length of the cell is increased, the modulation amplitude can exceed 70%. If we impressed a steady state or dc electric field on the electrodes half-way between 350 and 380 V/mm or 365 V/mm and applied a sinusoidal alternating or ac voltage with an amplitude of 30-V peak-to-peak, a sinusoidal modulation of the laser beam would occur. Digital modulation can be achieved by setting the steady field at 350 V/mm and applying a 30-V digital signal to switch the transmission of the cell between the 75% and 90% states.

3.3. Dielectric Waveguide Modulator

Normally Stark modulators are constructed from two parallel electrodes separated by a distance much smaller than the width to minimize the variation of the electric field across the laser beam. The electrodes are placed inside of a dielectric tube, typically glass or ceramic, held at a pressure appropriate for the gas used for modulation, typically a few torr. A typical spacing would be on the order of 2-mm with a width of 20 or more mm and a length of more than 200 mm. One of the problems with this design is that normal expansion of the laser beam through such a structure causes a loss of laser light due to vignetting of the beam by the electrodes. To reduce this vignetting loss, we have designed a Stark modulator using a hollow glass dielectric tube to confine the optical beam with minimum loss. The laser beam is focused into the proper size by a lens to form a match to the EH_{11} waveguide mode of the dielectric tube. A lens following the waveguide collimates the beam for propagation to a detector or to other optical components. The electrodes are external to the dielectric tube that serves to

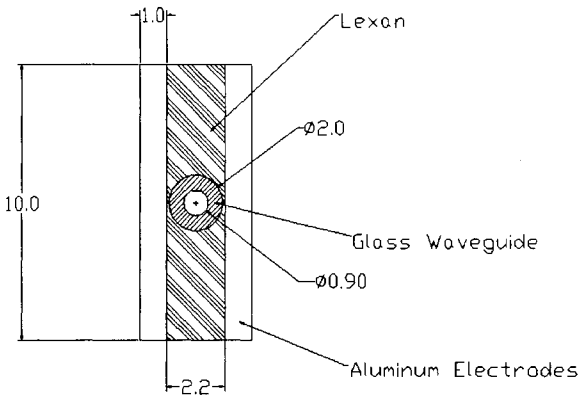

Fig. 7. End view of 0.9-mm i.d. glass modulator. All dimensions are in millimeters.

confine the optical beam and provide a means to operate the modulator at the reduced pressures required for operation.

To test this concept we constructed a 0.9-mm i.d. × 20-cm dielectric waveguide modulator. The waveguide material is borosilicate glass and is suspended between two 1-cm-wide by 20-cm-long flat aluminum electrodes. Lexan inserts are used to fill the gap between the electrodes outside of the waveguide. These Lexan inserts support the waveguide, align the electrodes and flatten and enhance the electric field in the waveguide. A sketch of the cross-section of the modulator is shown in Fig. 7. The ends of the waveguide we are sealed with ZnSe Brewster windows.

One problem that arises with this external electrode design is charge build-up from stray ions and electrons in the insulating waveguide. When an electric field is applied to the electrodes, the stray free charge in the waveguide migrates to the sides of waveguide nearest the electrodes with electrons attracted to the most positive electrode and ions attracted to the most negative electrode. This charge migration acts to cancel the electric field inside the waveguide thereby canceling modulation. We measured the time required for this canceling charge to build-up and found that it is on the order of or less than 1 sec. Because the charge build-up requires a finite time to occur, we have developed a biasing method that negates the effect of the stray canceling charge.

3.4. AC Biasing Method

The Stark components are created when an electric field is applied to the molecule. For the deuterated ammonia line that is in near coincidence with the 10.59-μm CO_2 laser line, the selection rules for absorption require that the electric field be applied perpendicular to the electric field of the optical beam. The polarity of the electric field is not important. For instance, if the electric field is applied with the positive electrode on the right and the negative electrode on the left or vice-versa, the absorption structure is not changed. The absorption for plus and minus M components are the same. The absorption is proportional only to the magnitude of the electric field, not direction, as long as the proper polarization relationship between the applied field and the field of

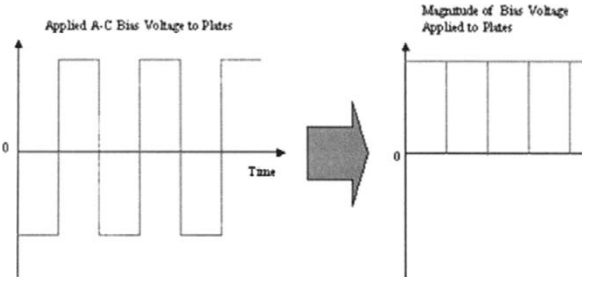

Fig. 8. The applied ac bias on the left produces the equivalent to a steady "dc" bias as shown on the right of the diagram.

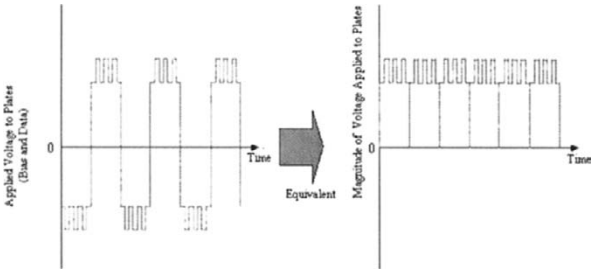

Fig. 9. The polarity of the data waveform must match the polarity of the bias waveform to properly modulate the laser beam.

the laser beam is maintained. Therefore a circuit has been developed that generates a low frequency (on the order of 100 to 1000 Hz) square wave that is applied to the electrodes. The waveform produced by the "ac bias" circuit is shown in Fig. 8. The polarity of the data waveform must match the polarity of the bias waveform to properly modulate the laser beam. This relationship is shown in Fig. 9. In addition the logic circuits buffer and temporally store the data and transmit the data waveform during the constant portion of the bias signal. High voltage amplifiers such as the Apex PA-94 have slew rates of approximately 1000 /μsec. Assuming a bias voltage level of 500 V and a bias frequency of 100 Hz, the switching transient will cause a duty cycle loss of only 0.05%. Using this type of biasing and data amplifiers, the waveform transmitted by the modulator should resemble the waveform shown in Fig. 10. The bandwidth of the modulator is limited only by the homogeneous linewidth of the deuterated ammonia gas. Using a filling pressure of 8-torr, a data rate of over 300-Mbits/sec is available.

4. Experimental Results

Using 0.9-mm i.d. $\times$ 20-cm dielectric waveguide modulator design discussed above and shown in Fig. 7, we measured the transmission of the modulator at pressures of 8, 11

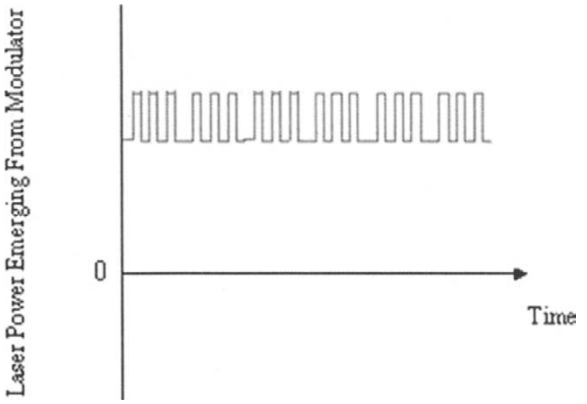

Fig. 10. The total waveform produced by the ac bias circuit combined with the data circuit appears identical to that produced using a dc bias voltage.

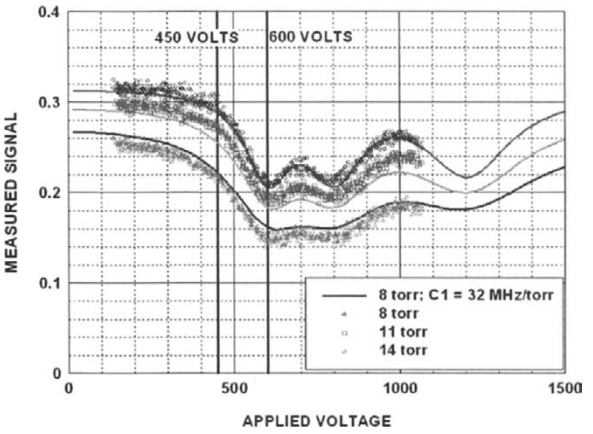

Fig. 11. The measured transmission of the 20-cm-long cell shows excellent agreement with theory.

and 14 torr as a function of the applied voltage. An "ac bias" waveform was generated by applying a square wave drive voltage from a signal generator to an iron-core step-up transformer (a 110 VAC to 6.3 VAC filament transformer operated in reverse). The bias was scanned from 0 to 1100 V peak and the transmitted signal was measured with a pyroelectric power meter. The "ac bias" frequency was 3000 Hz. The resulting modulator transmission as a function of applied voltage is shown in Fig. 11. The open circles are the measured data and the solid curves are the calculated transmission based on a theoretical model taking into account the cell length, pressure, e-field enhancement and deuterated ammonia fraction. The $M = 3$ and $M = 4$ absorption

peaks are clearly visible. The peak modulation index for this cell is approximately 30%. Using this information and verification of the model, we have designed and are constructing a 1-mm i.d. × 36-cm modulator for a prototype free-space optical link for high-speed digital transmission experiments.

References

1. 1996 HITRAN Molecular Line Database, U.S. Air Force.
2. HITRAN-PC, version 2.51, distributed by Ontar Corporation.
3. M.V. Berry and I.C. Percival, "Optics of fractal clusters such as smoke," Optica Acta **33**, 5 (1986).
4. P. Chylek, V. Ramaswamy, R. Cheng, and R.G. Pinnick, "Optical properties and mass concentration of carbonaceous smokes," Appl. Opt. **20**, 17 (1981).
5. D.B. Rensch and R.K. Long, "Comparative studies of extinction and backscattering by aerosols, fog, and rain at 10.6 μ and 0.63 μ," Appl. Opt. **9**, 7 (1970).
6. V. Chimelis, "Extinction of CO_2 laser radiation by fog and rain," Appl. Opt. **21**, 18 (1982).
7. C.J. Walsh, "An rf excited circular waveguide CO_2 laser," Rev. Sci. Instrum. **61**, 9 (Sept. 1990).
8. A.R. Johnston and R D.S. Melville, "Stark-Effect Modulation of a CO_2 Laser by NH_2D," Appl. Phys. Lett. **19**, 12 (1971).